Upper Colorado River streamflow dependencies on summertime synoptic circulations and hydroclimate variability

Zachary F. Johnson,[a] Jacob Stuivenvolt-Allen,[b] Hayden Mahan,[c] Jonathan D.D. Meyer[d,e]
Matthew Miksch [d,f]

[a] *Department of Earth and Atmospheric Science, Central Michigan University, Mt. Pleasant, Michigan, USA*
[b] *Department of Earth and Planetary Sciences, Yale University, New Haven, Connecticut, USA*
[c] *National Weather Service, Salt Lake City, Utah, USA*
[d] *Department of Plants, Soils, and Climate, Utah State University, Logan, Utah, USA*
[e] *Utah Climate Center, Utah State University, Logan, Utah, USA*
[f] *Department of Civil and Environmental Engineering, University of California - Davis, Davis, California, USA*

Corresponding author: Zachary F Johnson, johns1zf@cmich.edu

ABSTRACT: The southwestern United States is highly sensitive to drought, prompting efforts to understand and predict its hydroclimate. Oftentimes, the emphasis is on wintertime precipitation variability, yet the southwestern United States exhibits a summertime monsoon where a significant portion of annual precipitation falls through daily convection activities manifested by a mid-tropospheric ridge of high pressure. Here, we examine synoptic patterns of the southwestern ridge through a k-means clustering analysis and assess how these synoptic patterns translate into streamflow changes in the upper Colorado River basin. A linear perspective suggests $\sim 17\%$ of upper Colorado River discharge at Lee's Ferry, Arizona gauge comes from summertime monsoon rains. The ridge of high pressure exhibits diversity in its intensity, structure, and position, inducing changes in moisture advection and precipitation. A ridge shifted north or east of its climatological center increases moisture and precipitation over the southwestern United States, while a ridge toward the south or northwest inhibits precipitation. A ridge east of its climatological center contributes to increased streamflow, whereas a ridge west or northwest of its climatological center decreases streamflow. Cooling in the central tropical Pacific and the Pacific Meridional Mode region favors an eastward shift of the ridge of high pressure corresponding to wet days. Eastern tropical Pacific warming favors a southward shift of the ridge corresponding to dry days. These results support an intermediate scale between climate forcing and summertime Colorado River discharge through changes in the intensity, structure, and position of the southwestern ridge of high pressure, integral to the Southwest United States hydroclimate.

1. Introduction

In recent years, the semiarid Intermountain West and southwestern United States have undergone long-lasting droughts, threatening vital water resources that support a wide range of industrial sectors, human health, and ecosystems (Cook et al. 2010; Pederson et al. 2012; Cook et al. 2015; Seager et al. 2015; Mankin et al. 2021; Williams et al. 2022). Given most cold season precipitation is stored as snowpack, research efforts have been directed to understand the climate factors leading to changes in wintertime precipitation and how they translate to river discharge (Erb et al. 2020; Chikamoto et al. 2020; McCabe et al. 2020; Stuivenvolt-Allen et al. 2021). Yet, a significant portion of annual precipitation also falls in the summertime due to the North American Monsoon (NAM) (Higgins et al. 1997, 1999; Cerezo-Mota et al. 2011). During spring snow melt, the Colorado River exhibits increased discharge rates from early spring through early summer prior to the onset of the NAM. Once NAM activates, a question remains whether a favorable summertime synoptic pattern accompanying increased precipitation will help offset reducing discharge rates (Carroll et al. 2020). Here, we attempt to fill a knowledge gap between climate variability and Colorado River discharge by emphasizing summer synoptic circulation changes, given monsoon rains can contribute to $\sim 10\%$ of annual Colorado River streamflow.

The NAM is a seasonal change of the large-scale atmospheric circulation that promotes increased precipitation in the southwestern United States and northern Mexico during the summer (Douglas et al. 1993; Adams and Comrie 1997; Higgins et al. 1999; Barlow et al. 1998). It is manifested through a mid-tropospheric subtropical ridge of high pressure that establishes itself in late May and June over northern Mexico and the southwestern United States, which corresponds to warming surface air temperatures (Hales Jr 1972; Erfani and Mitchell 2014; Seastrand et al. 2015). As such, the land–ocean temperature gradient increases, inducing moist airflow from the warm Gulf of California and the Gulf of Mexico toward the Desert Southwest region (Douglas 1995; Bieda et al. 2009; Hu and Dominguez 2015). Increased humidity leads to an unstable atmosphere, resulting in a pronounced diurnal cycle in atmospheric convection. As a result, daily thunderstorm activity over the Desert Southwest occurs mid-June through August (Fuller and Stensrud 2000; Finch and Johnson 2010). The NAM decays in September as midlatitude jet stream activities subside the ridge of high pressure. Because the NAM involves land-atmosphere and ocean-atmosphere effects, changes in the structure, intensity, and location of the mid-tropospheric ridge of high pressure drive changes in winds, moisture transport, and precipitation.

A limited number of research articles indicate that variability of the southwestern mid-tropospheric high pressure system (and hence the NAM) may be linked to low-frequency climate variability (D'Arrigo and Jacoby 1991; Brown and Wu 2005; Sagarika et al. 2016; Kim et al. 2008; Peltier and Ogle 2019; Zhao and Zhang 2022). For instance, the El Niño-Southern Oscillation (ENSO) atmospheric teleconnection stems from a quasi-stationary Rossby wave train emanating from the western tropical Pacific. An El Niño favors a southward shift in the mid-tropospheric high pressure system leading to dry conditions, while the opposite is true for a La Niña (Demaria et al. 2019). SST variability in the adjacent Pacific Ocean (Gulf of California) or the Gulf of Mexico may also induce regional wind shifts and changes in humidity necessary for monsoonal moisture to reach the southwestern United States. Alternatively, the Madden-Julien Oscillation (MJO) may impact the NAM by amplifying easterly waves in the eastern North Pacific and promoting tropical cyclone genesis, which fosters moisture surges toward northern Mexico and the southwestern United States (Lorenz and Hartmann 2006).

Here, we examine variability in structure, intensity, and location of the mid-tropospheric high pressure system associated with the NAM to assess which synoptic patterns favor increased or decreased precipitation over the upper Colorado River basin, and then link them to changes in upper Colorado River streamflow and climate variability. Our principal research questions are:

1. How does the location, structure, and intensity of the southwestern ridge of high pressure accompany precipitation changes during the NAM?
2. How do Pacific Ocean teleconnections and climate patterns affect the location, structure, and intensity of the southwestern ridge of high pressure?
3. Can the relationship between the location of the southwestern ridge of high pressure and upper Colorado River streamflow be quantified?

To answer these questions, we first statistically decompose the July–August 500 hPa ridge of high pressure over the southwestern United States through a k-means clustering method of daily 500 hPa geopotential height. Next, we reveal which k-means clusters favor positive and negative precipitation anomalies in the upper Colorado River basin and the Desert Southwest based on the structure, intensity, and location of the 500 hPa ridge of high pressure. We then aggregate the 500 hPa patterns that favor positive or negative precipitation in the upper Colorado River basin and assess whether there is a significant change in discharge rates. The aggregated composite k-means also favor modes of climate variability. We detail the k-means clustering technique in Section 2. Then we describe our results of the k-means clustering of the 500 hPa ridge of high pressure in Section 3, link it to climate variability in Section 4, and examine its dependencies on upper Colorado River streamflow in Section 5. We end with a discussion with concluding remarks in Section 6.

2. Data and methods

a. Reanalysis data

To link variability in the southwestern ridge of high pressure to precipitation, we obtain ERA5 daily 500 hPa geopotential height (Z500), ERA5 daily lower-tropospheric winds (UV850), and ERA5 total column precipitable water (PWAT), which comprises of vertically integrating 37 levels (Hersbach 2016). These ERA5 datasets have $0.25° \times 0.25°$ resolution. We also obtain daily Climate Prediction Center Merged Analysis of Precipitation (CMAP) Global Unified Guage-Based Analysis of Daily Precipitation, which has a $0.25° \times 0.25°$ resolution (Xie et al. 2007; Chen et al. 2008) in the United States and a $0.5° \times 0.5°$ resolution worldwide (Xie et al. 2010). For daily precipitation anomalies, we quantify area-averaged precipitation constrained only to the upper Colorado River basin by constraining grid points within the upper Colorado River basin boundary (Fig. 1). From these variables, we calculate daily anomalies based on the 1980–2020 mean. For monthly data, we obtain COBE-SST ($1° \times 1°$ resolution) (Ishii et al. 2005) and ERA5 Z500 ($0.25° \times 0.25°$ resolution) (Hersbach 2016) products and compute monthly anomalies based on the 1980–2020 mean. The following analysis is constrained to the July–August period for daily and monthly anomalies. The linear trends at each grid point are extracted from the anomalies to remove the long-term trend, such as the global warming component.

b. Modes of Climate Variability

To assess the dependencies of climate variability and the southwestern ridge of high pressure, we calculate the Niño3, Niño4, and Pacific Meridional Mode time series. The Niño3 and Niño4

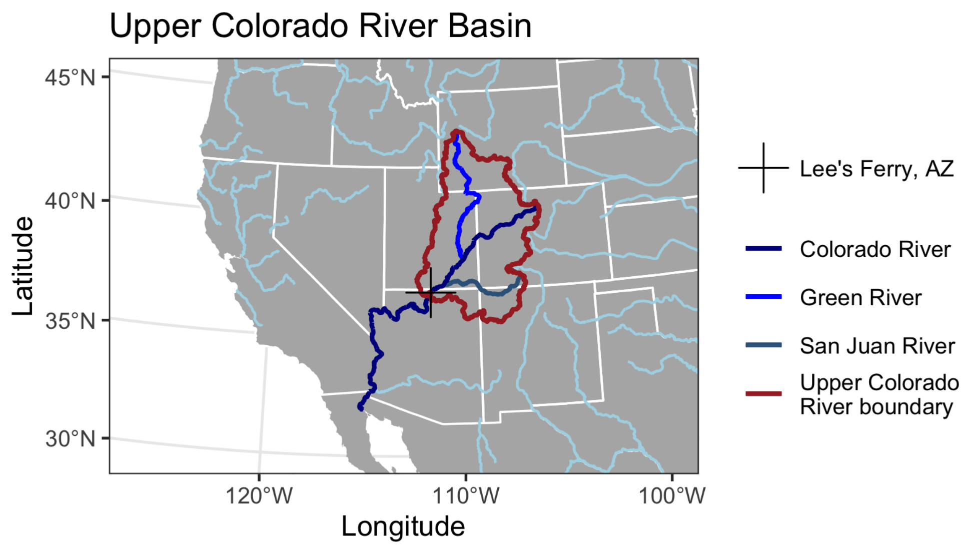

FIG. 1. Upper Colorado River Basin in brown, with the Colorado River in dark blue. The two other major rivers in the basin are the Green River (north) and the San Juan River (south). The Lee's Ferry, Arizona gauge is denoted by the cross at the southwestern edge of the upper Colorado River basin. Other major rivers are denoted in light blue.

time series are computed by the area average of SST anomalies in the eastern tropical Pacific (5°S–5°N, 150°W–90°W) and central tropical Pacific (5°S–5°N, 160°E–150°W). The Pacific Meridional Mode is the leading mode by applying singular value decomposition between SST anomalies and 10-m UV wind vectors in the northeast tropical Pacific (21°N–32°N, 74°W–15°E) (Chiang and Vimont 2004).

c. Colorado streamflow data

We obtain monthly and daily Colorado streamflow data at Lee's Ferry, Arizona, USA for the 1980–2019 and 1980–2020 periods from the United States Department of Interior's Bureau of Reclamation and the United States Geological Survey (USGS) (Topping et al. 2003; U.S. Department of Interior 2020). Lee's Ferry is at the drainage region of the upper Colorado River Basin (outlined in brown in Fig. 1). This Upper Colorado River Basin comprises southwest Wyoming, eastern Utah, western Colorado, northeastern Arizona, and northwestern New Mexico, and has two major rivers that feed into the Colorado River: the Green River and the San Juan River. More than 90% of the natural streamflow in the upper Colorado basin passes through Lee's Ferry. As such, we chose to perform our analysis at this location.

There are many reservoirs and dams upstream of the Lee's Ferry gauge for water storage and hydroelectric power, so the USGS implements a hydrological model that adjusts raw streamflow to compensate for human activities (U.S. Department of Interior 1983). As a result, naturalized streamflow data are computed by removing these anthropogenic impacts (i.e., reservoir regulation, reservoir evaporation, irrigated agriculture, water consumption) from the raw recorded historical flows (Prairie and Callejo 2005). These data are developed and updated regularly by the Bureau of Reclamation. Naturalized streamflow data is only available in a monthly format; therefore, we also extend our analysis to raw daily streamflow without anthropogenic effects removed, obtained from the USGS.

Daily timescale streamflow at the outlet of the upper Colorado River basin lags monsoon rains and runoff upstream of the Lee's Ferry gauge. Past research indicates that the streamflow response time from precipitation is dependent on many variables, such as season, soil moisture, soil characteristics, land cover, geological porosity, precipitation duration, and precipitation location (Orth and Seneviratne 2013; Hrachowitz et al. 2013; Bizuneh et al. 2021). One study assessed this lagged relationship on a sub-basin of the upper Colorado River at the Colorado Headwaters Basin and determined during summer the lagged precipitation relationship was about 1 day (Franzen et al. 2020). Another study found that most rivers in the Intermountain West have a 1- to 3-day lag (Moges et al. 2022). To account for the large basin (drainage area), our study applies a 5-day streamflow mean (days 0–4) following daily precipitation (day 0) for raw daily streamflow. As a result, the gauge at Lee's Ferry will partially represent the integration of the previous 5-days precipitation for the raw daily streamflow analysis.

d. K-means cluster analysis

To statistically decompose the mid-tropospheric southwestern ridge of high pressure into preferred synoptic patterns, we apply k-means clustering on the daily 500 hPa geopotential height (Z500) field over the western United States through July–August from 1980–2020 (20°N–45°N, 90°W–145°W) using the Hartigan and Wong (1979) AS-136 algorithm. The k-means clustering method decomposes data into k clusters based on the intracluster variance of the squared Euclidean

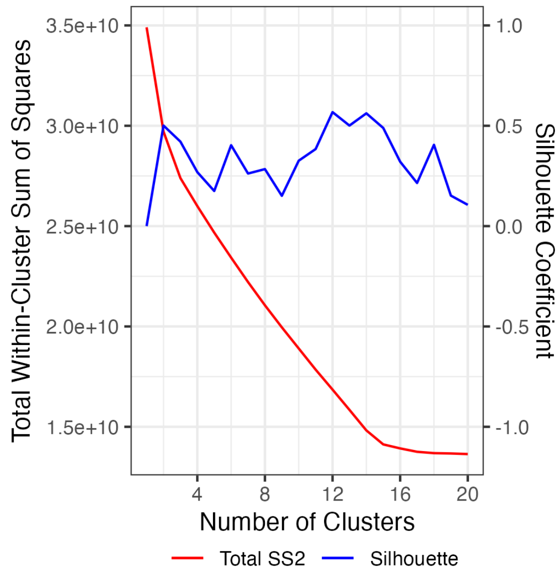

FIG. 2. Total within-cluster sum of squares (left y-axis) and Silhouette coefficient (right y-axis) for n clusters 1–20.

distance between data points (Milligan and Cooper 1985; Gong and Richman 1995; Jolliffe and Philipp 2010; Jain 2010; Govender and Sivakumar 2020). In other words, the k-means algorithm groups daily synoptic patterns that are similar to one another.

One of the challenges in the k-means clustering analysis is obtaining an optimal number of clusters. When datasets exhibit evident and obvious separate patterns, as observed for midlatitude circulations associated with low-frequency climate variability, the optimal number of clusters may be clearly defined in the data. However, summer synoptic circulations in the western United States are primarily dominated by a subtropical ridge of high pressure that accompanies subtle variations in location, structure, and strength, inhibiting clearly defined synoptic regimes. To determine the optimal number of summertime synoptic patterns, we apply the "elbow" and the "silhouette" methods proposed by Kodinariya et al. (2013). First, we repeat the k-means procedure from clusters 1–20 (k). Next, we plot the total within-cluster sum of squares against the k number of clusters and visually look for the "elbow" in the curve (red line in Fig. 2). Alternatively, the "silhouette" method measures the compactness and separation between the k clusters by quantifying how close each element of one cluster is to the elements of the neighboring clusters (Rousseeuw 1987). Greater silhouette coefficients indicate better the classification of synoptic patterns (blue line in Fig. 2).

The total within-cluster sum of squares curves for the initial 1–3 k clusters, then follows a quasi-linear line from clusters 4 through 14, and finally deviates significantly after cluster 15, thereby indicating the ”elbow” is located at cluster 15 (Fig. 2). Arguably, k clusters of 2 suggest an ”elbow,” but past research on the southwestern ridge of high pressure indicates more than three summertime patterns in the southwestern United States and northern Mexico (Diem and Brown 2009; McCann 2010; Mazon et al. 2016). The silhouette coefficient exceeds 0.5 at clusters 2, 12, 13, and 14, with the greatest values for clusters 12 and 14 (~ 0.52). Based on the two methods, an optimal number of clusters is between 12–15, and here we apply $k = 15$ clusters. These 15 clusters represent changes in the intensity, structure, and position of the summertime southwestern ridge of high pressure. We organize the clusters in descending order based on the Upper Colorado River Basin anomalous precipitation (e.g., cluster 1 corresponds to the highest anomalous precipitation and cluster 15 the lowest).

3. Summertime southwest synoptic variability

a. July–August Climatology

The July–August synoptic conditions are dominated by a mid-tropospheric ridge of high pressure centered over New Mexico (Fig. 3c). A significant portion of precipitation occurs over the Desert Southwest as depicted in Figure 3a. Over northwest Mexico, including the states of Sonora, Sinaloa, Chihuahua, and Durango, over 50% of annual precipitation falls in July–August due to the NAM. This percentage decreases to the north, yet still, a significant portion of annual precipitation falls during July–August in far southeastern California and Nevada, Arizona, and New Mexico (20–40%). Additionally, 10–20% of annual precipitation falls in Utah and Colorado during these two months. The percentage decreases over northern Utah, northern Colorado, and Wyoming. However, increased terrain-based precipitation over Utah, Colorado, and Wyoming is evident over the upper Colorado River basin in Figure 3a. We see a significant portion of precipitation over the central and northern Great Plains, but much of that precipitation is in the form of mesoscale convective systems cresting the mid-tropospheric ridge of high pressure, not necessarily directly related to the NAM (Houze Jr 2004; Wang et al. 2011; Houze Jr 2018). In the upper Colorado River basin, an estimated 22% of annual precipitation falls in July–August by quantifying the basinwide

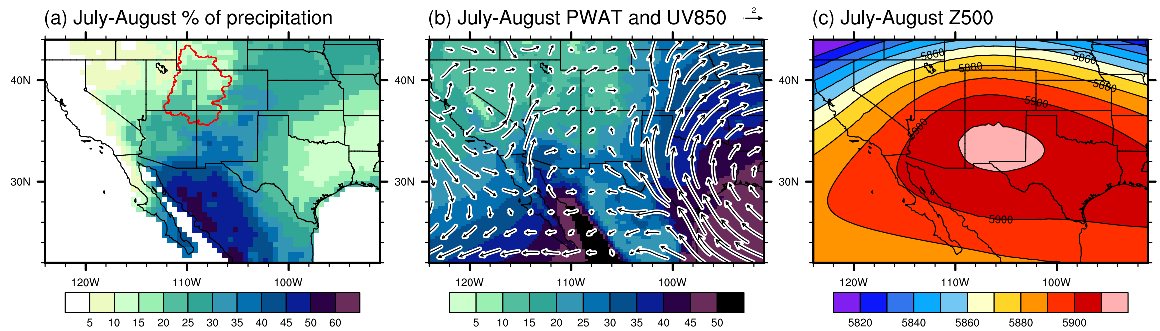

FIG. 3. (a) 1980–2020 July–August percent of annual precipitation (%) with the Upper Colorado River boundary (red), (b) July–August climatoloigcal PWAT (kg/m^2) and UV850 (m/s), and (c) July–August climatological Z500 (m).

area average. As a result, a large portion of annual precipitation falls during July–August over the southwest USA.

Figure 3b depicts climatological PWATs, characterized by a moist atmosphere over the Gulf of California and the Gulf of Mexico. Lower-tropospheric winds show climatological southerlies over the southern Great Plains with an easterly component over Texas, advecting moist air toward the southwestern United States, typically east of the Sierra Madre Mountains and the Continental Divide. Additionally, a weak climatological southwesterly wind component over the Gulf of California fosters moisture advection towards the southwestern United States. The NAM is usually in the form of periodic moisture plumes through low-level jets due to a favorable synoptic environment, so to assess the NAM, one method is assessing the eddy moisture flux to quantify these transient perturbations (Arritt et al. 2000; Favors and Abatzoglou 2013). Alternatively, we can examine daily k-mean clusters that categorize synoptic patterns and then see how those synoptic patterns characterize changes in lower-tropospheric winds, atmospheric moisture, and precipitation, illustrating transient perturbations in the large-scale pattern.

b. Cluster analysis of 500 hPa heights

Figure 4 shows the 15 k-means clusters depicted by 500 hPa geopotential height anomalies. Note that the July–August climatological mean high pressure center is over New Mexico (Fig. 3c). Figure 4 depicts significant variability in the location, intensity, and structure of the southwestern ridge of high pressure. Clusters 1–3 depict an anomalous dipole consisting of positive Z500 anomalies over

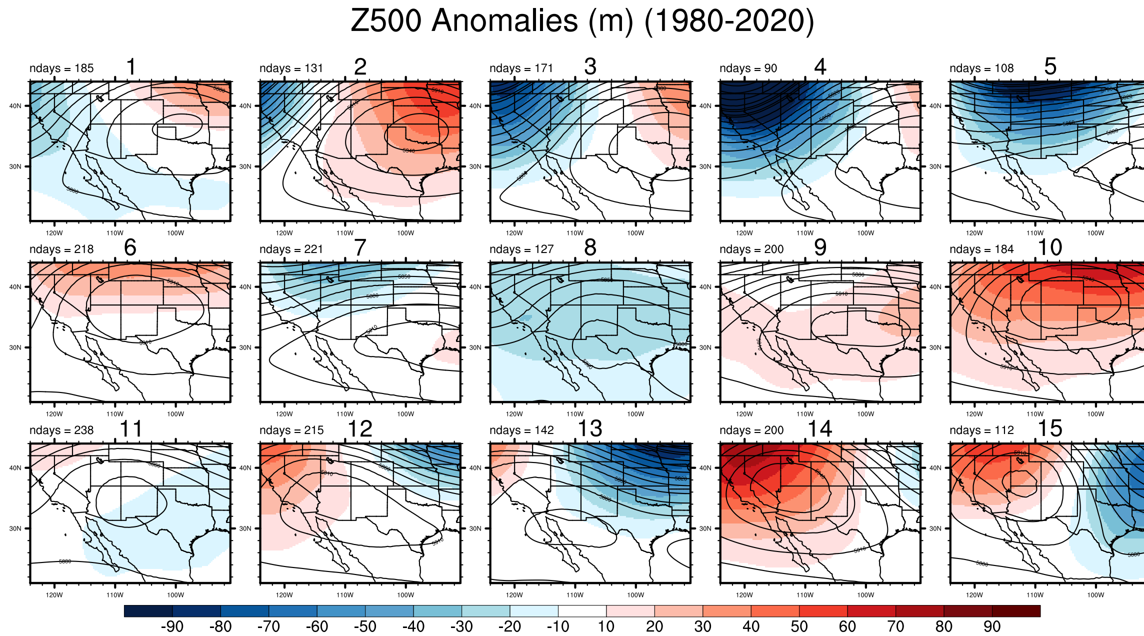

FIG. 4. k-mean cluster analysis of detrended daily (contours) 500 hPa geopotential height and (colors) 500 hPa geopotential height anomalies from July–August (1980–2020) over the southwestern United States and northern Mexico (20°N–45°N, 90°W–145°W). The number of days for each k-means is on the top left of each subplot.

the Great Plains of the United States and negative Z500 anomalies over the western United States (Fig. 4). It follows that Clusters 1–3 characterize the ridge of high pressure east of its climatological position. Clusters 4 and 5 are characterized by negative Z500 anomalies over the western United States, illustrating troughing over the Upper Colorado River. Clusters 6 and 10 show anomalous positive Z500 anomalies over the northern United States (Fig. 4), characterized by the ridge of high pressure shifted north of its climatological mean. Clusters 12–15 show the opposite dipole as clusters 1–3, consisting of negative Z500 anomalies over the eastern half of the United States and negative Z500 anomalies over the western half. Notably, clusters 14–15 depict negative Z500 anomalies centered over the northwestern United States, thereby characterizing the ridge of high pressure northwest of its climatological position (Fig. 4). This diversity in the location, intensity, and structure of the 500 hPa ridge of high pressure triggers a response in lower- to mid-tropospheric winds, moisture, and precipitation.

The different clusters of mid-tropospheric circulations result in a range of precipitation anomaly patterns in and around the upper Colorado River basin (Fig. 5). Clusters 1–4 favor wetting across most of the upper Colorado River basin, whereas clusters 5–8 show north-south contrasts

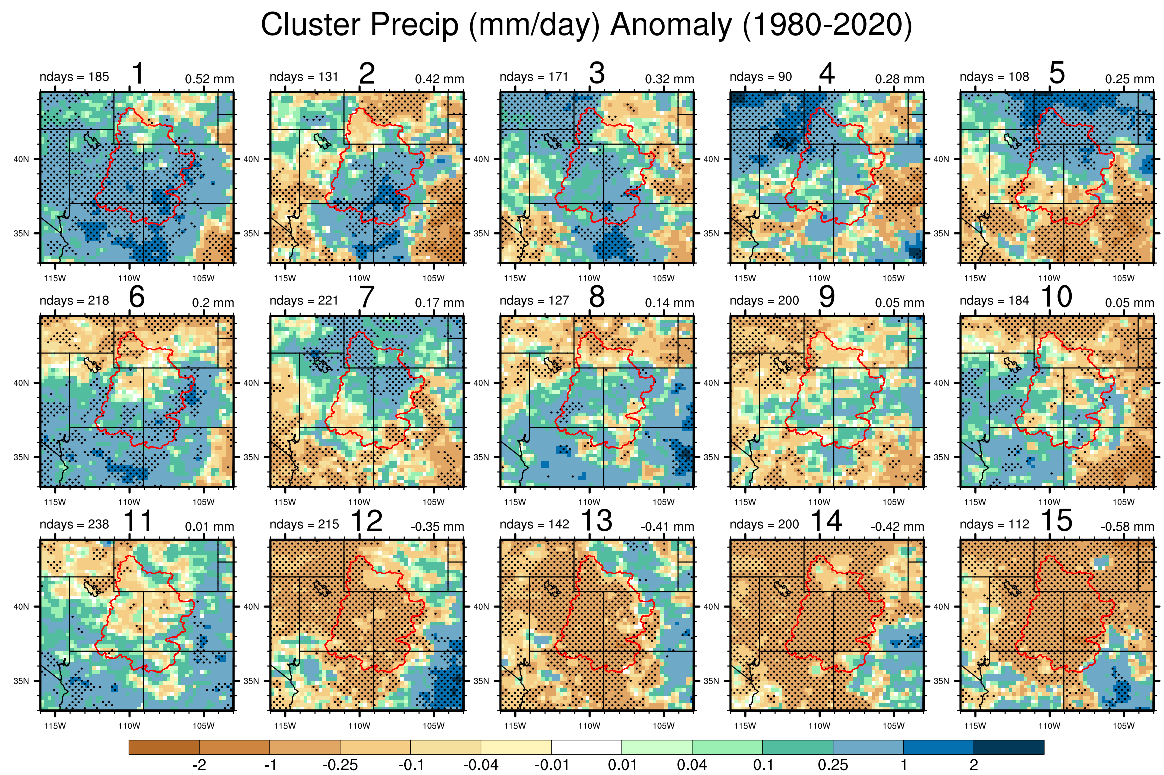

FIG. 5. CPC Precipitation anomalies (mm/day) associated with each cluster in Figure 4. Note the color bar has a logarithmic ramp. The Upper Colorado River is outlined in red and the basin area-averaged precipitation anomaly is on the top right of each subplot. The dotted region shows above the 90% statistical significance level using Student's t-test for precipitation anomalies against corresponding Z500 cluster in Figure 4.

of precipitation anomalies within the upper Colorado River Basin, yet basinwide, they are still anomalously wet. Clusters 9–10 show local variations in precipitation anomalies, favoring slight wetting. Cluster 11 is near normal basin-wide. Clusters 12–15 are anomalously dry basinwide.

Interestingly, the synoptic patterns that favor a wetting pattern in the upper Colorado River basin show similarities in the structure and position of the 500 hPA ridge of high pressure (Fig. 5 and Fig. 4). Cluster 1–3 (19.2% of days) depict the ridge of high pressure shifted east of its climatological center, whereas Cluster 4 and 5 (7.8%) indicate troughing. Clusters 12–15 show the ridge west of its climatological mean (26.3% of days). Notably, the driest clusters (12,14, and 15) depict the ridge of high pressure northwest of its climatological mean (20.7% of days). Cluster 13 depicts the ridge of high pressure south of its climatological mean (5.6% of days). We summarize and categorize these clusters based visual assessment of the ridge of high pressure location obtained by the k-means algorithm in Table 1. These results suggest that a ridge of high pressure favoring a wetting pattern over the upper Colorado River basin is typically east of the climatological mean, whereas a ridge of high pressure favoring a drying pattern is toward the west of the climatological mean, with the northwest position being the driest.

TABLE 1. Summary of preferred synoptic patterns of the 500 hPa ridge of high pressure based on position, classification whether they are wet or dry in the upper Colorado river basin, cluster numbers, the percent of July–August days in 1980–2020, and area-averaged precipitation anomalies (mm/day) constrained in the upper Colorado River basin outlined in Figure 1.

Ridge position	Classification	Cluster	% of days	Precip anomaly mm/day
East	Wet	1,2,3	19.2%	+0.42
Trough	Wet	4,5	7.8%	+0.26
North	Wet	6,10	15.8%	+0.13
–	Neutral	7,8,9,11	21.6%	+0.07
South	Dry	13	5.6%	-0.41
West/Northwest	Dry	12,14,15	20.7%	-0.43

Generally, the ridge of high pressure structure, location, and intensity can control lower-tropospheric flow and hence, changes in atmospheric moisture content. Figure 6 shows PWAT anomalies based on the percentage from its climatological mean and 850 hPa wind vectors for each cluster's days. Similar to the precipitation anomaly patterns (Fig. 5), each cluster depicts different patterns of PWAT anomalies and UV850 winds characterizing the transient nature of the NAM. Clusters 1–3 show lower-tropospheric southeasterly winds curving southwesterly at the western periphery of the mid-tropospheric ridge of high pressure that accompany anomalously positive PWATs over the Upper Colorado River basin and regionally over the southwestern United States. Additionally, clusters 1–3 depict a lower-tropospheric anticyclonic circulation over the Arkansas-Louisiana-Texas region, funneling moisture from the Gulf of Mexico toward the Sierra Madre Mountains and the Continental Divide. This lower-tropospheric anticyclone compliments an eastward placement of the 500 hPA ridge of high pressure that favors a wet pattern (Fig. 4). Notably, Cluster 1 shows a weaker horizontal pressure gradient extending to the west coast of the United States compared to Clusters 2 and 3 (Fig. 4), which minimizes dry air advection from the colder waters adjacent to the California and Oregon coasts.

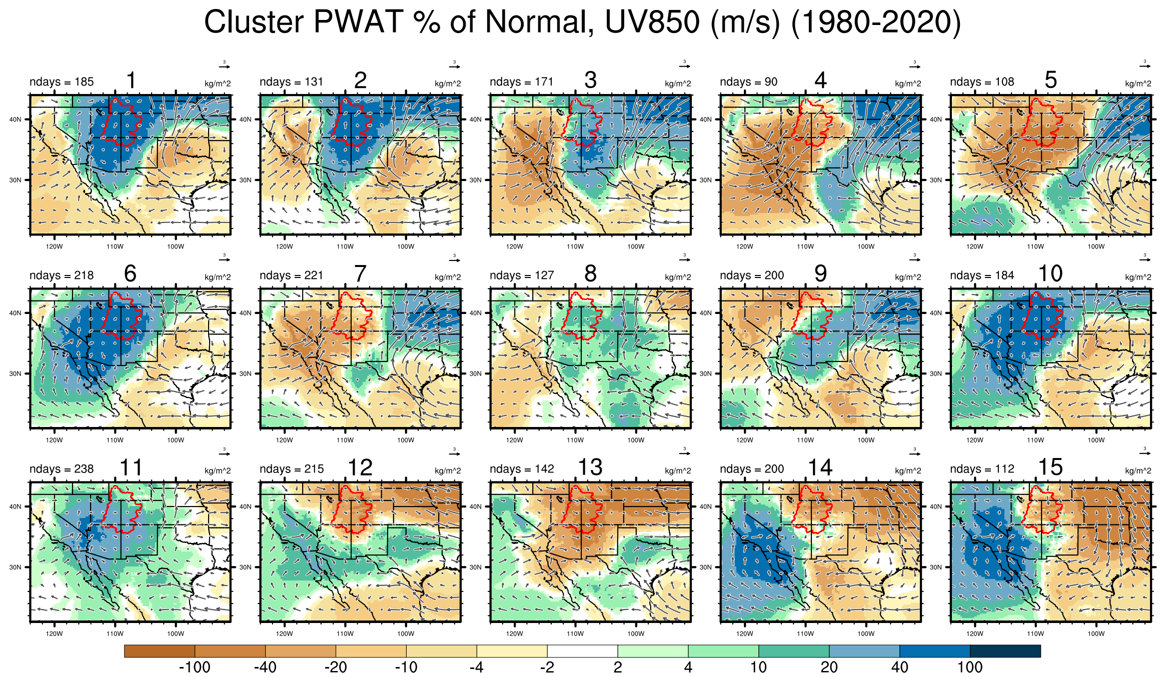

FIG. 6. PWAT percent from normal (colors) and UV850 winds (arrows) associated with each cluster in Figure 4. The Upper Colorado River is outlined in red.

Clusters 4 and 5, characterized by troughing over the upper Colorado River basin, show anomalously negative PWATs (Fig. 6). The troughing pattern in Clusters 4 and 5 coincide with lower-tropospheric northwesterly and westerly winds over California and the adjacent Pacific Ocean, inhibiting atmospheric moisture over the Upper Colorado River basin. Also, the southeasterly to southwesterly winds from the Gulf of Mexico inhibit moisture advection to the uppper Colorado River basin. Therefore, the positive precipitation anomalies in Clusters 4 and 5 are primarily forced by mid-latitude cyclones rather than a favorable ridge of high pressure pattern that advects moisture toward the basin. Meanwhile, Clusters 6 and 10, characterized by a ridge of high pressure north of its climatological mean, depict robust positive PWAT anomalies over the Upper Colorado River basin extending towards the Baja California peninsula. Cluster 6 and 10 also favor positive precipitation anomalies, but primarily over the southern part of the Upper Colorado River basin.

Synoptic patterns that favor a dry pattern over the upper Colorado River basin (clusters 12–15) are characterized by negative PWAT anomalies over the upper Colorado River basin. Clusters 12, 14, and 15, characterized by a ridge of high pressure west or northwest of its climatological position, coincide with lower-tropospheric northwesterly winds over the upper Colorado River basin. Accompanying these northwesterly winds, atmospheric moisture is shifted over California, Nevada, and Arizona. Cluster 13, characterized by ridge of high pressure south of its climatological mean, also depicts lower-tropospheric northwesterly winds and negative PWAT anomalies over the basin. Notably, these dry clusters for the Upper Colorado River basin do not necessarily correspond to a dry Arizona, New Mexico, or Mexico (Fig. S1). Yet, the structure of the ridge of high pressure being toward the south or northwest in clusters 12–15 generally supports a synoptic pattern that limits moisture advection to the Upper Colorado River basin (Fig. 4).

4. Southwestern ridge of high pressure dependencies on climate variability

Previous research suggests that La Niña conditions promote an active monsoon due to a northward shift of the monsoon ridge (Castro et al. 2001). We aggregate the five obvious changes in location of the mid-tropospheric ridge of high pressure obtained from the k-means in Figure 4: toward the east promoting wetting, to the north promoting wetting, toward the south promoting drying, toward the west/northwest promoting drying, and troughing promoting wetting (Fig. 7 and Table 1). Interestingly, 1982, 1983, and 2003 were the only years with >= 20 days where the k-mean favored the ridge of high pressure directly north of its climatological mean. The 1982–1983 years featured a transition to a strong El Niño, followed by a La Niña, characterized by the positive SST anomalies in the eastern tropical Pacific in Figure 8e. Notably, the k-means depicting active monsoon days in its northern extent (upper Colorado River basin) is primarily due to an eastward shift in the southwestern ridge of high pressure (Table 1). During the years 1999, 1983, 1995, 1980, and 2011, more than 30% of July–August days favored a ridge of high pressure to the east (Fig. 8a). It is characterized by negative Z500 anomalies over the northeast Pacific, positive anomalies over the Intermountain West, and negative anomalies over the east coast of the United States. This eastward shift of the southwestern ridge of high pressure accompanies robust cooling in the central tropical Pacific to Baja California, corresponding to La Niña-like conditions and an anomalously cool Pacific Meridional Mode (PMM) region (Figs. 8a and 2S). The frequency of days in July–August characterized by an eastward shift in the ridge of high pressure has dependencies on Niño4 and the PMM SST anomalies ($R = -0.43, p = 0.005$ and $-0.45, p = 0.004$). Alternatively, July–August positive precipitation anomalies may be related to an active negative Pacific-North

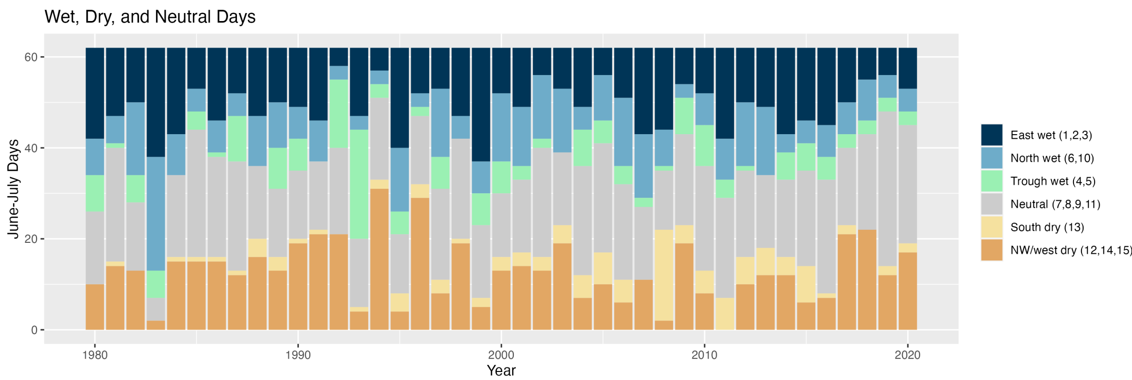

FIG. 7. The number of days where the ridge of high pressure is shifted east, north, south, and northwest, and days where there is a trough of low pressure, obtained by the k-means in Figure 4 and 5. The cluster number is noted on the legend.

America pattern that accompanies troughing over the Upper Colorado River Basin, yet there is no obvious link to Pacific SST anomalies (Fig. 8c).

When the ridge of high pressure is northwest of its climatological position for 40% of July–August days in 1994, 1996, 2018, 1991, and 2017, no robust climate variability is evident (Fig. 8b). The frequency of July–August days with a northwestward shift is weakly correlated with the PMM: $R = 0.36, p = 0.025$. However, the southward shifted ridge of high pressure based on its climatological position favors an eastern Pacific El Niño (Fig. 8d), accounting for 24% of July–August days in 2008, 2015, 2005, and 2011 consistent with past research (Demaria et al. 2019). The frequency of July–August days with a southward shift of the ridge of high pressure correlates with Niño3 SST anomalies ($R = 0.44, p = 0.008$). For these years, negative Z500 anomalies emerge over the southwestern United States, indicative of a southward shift in the ridge of high pressure (Fig. 8). These results point to the remote ocean effect on preferred daily synoptic patterns of the 500 hPa ridge of high pressure.

Previous research suggests an atmospheric teleconnection for the NAM when the MJO is in its active phase in the Indian Ocean (Lorenz and Hartmann 2006). Clusters 1, 5, 6, 8, 11, 13 show days favoring an active MJO phase two in the Indian Ocean in Figure S3, but that does not necessarily correspond to a wet upper Colorado River basin (Fig. S1). These same clusters depict robust positive precipitation anomalies over Mexico, supporting past research linking the MJO phase 2 to an active NAM over Mexico. They do not depict any consistent ridge of high pressure

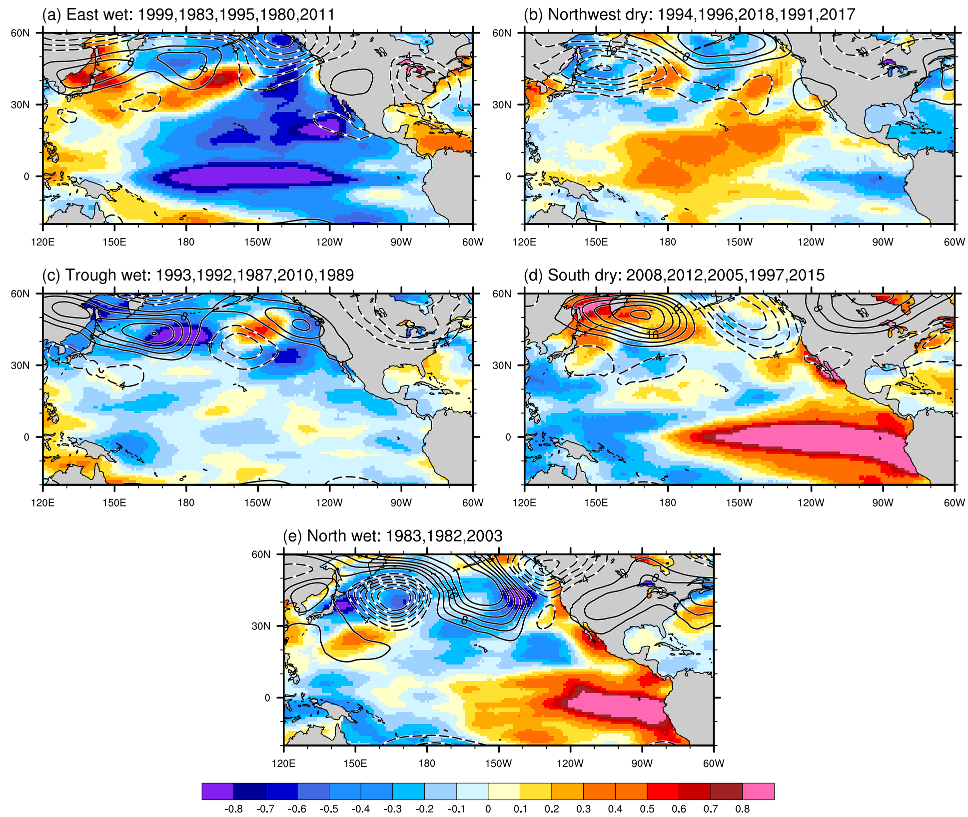

FIG. 8. SST and Z500 anomalies based on July–August seasons favoring synoptic patterns where the ridge of high pressure is shifted (a) east, (b) northwest, (d) south, and (e) north, and a (c) troughing pattern obtained by the k-means clusters in Figure 4. Z500 geopotential height (m) are in increments of 4 m with the zero contour omitted.

synoptic pattern. Rather, this study finds changes in the ridge of high pressure synoptic patterns are associated with remote ocean forcing such as ENSO or internal variability.

Note that a correlation coefficient more robust than ±0.34 is statistically significant at the 95% level when considering the effect of autocorrelation of climate variability (Bretherton et al. 1999). As a result, the above correlation coefficients aforementioned are statistically significant.

5. Changes in Colorado River streamflow

Based on the synoptic variability of the southwestern ridge of high pressure, we examine their dependencies on naturalized monthly and raw daily streamflow for the upper Colorado River at the Lee's Ferry, Arizona gauge through precipitation changes.

a. Naturalized monthly streamflow

First, we decompose the monthly naturalized streamflow (1980–2019) at the Lee's Ferry, Arizona gauge into seasonal and trend components in Figure 9 (Cleveland et al. 1990; Cavadias 1994; Vaheddoost and Aksoy 2019). The naturalized streamflow exhibits strong seasonality, with increased discharge in spring and summer due to snow melt from cold season precipitation (Fig. 9a). Notably, a negative trend in upper Colorado River discharge has emerged in the past 40 years, prompting efforts to understand the upper Colorado River hydroclimate (Fig. 9c). We remove the seasonal component in the monthly naturalized streamflow in Figure 9e, and perform the following analysis with this data. A close relationship exists between upper Colorado River discharge and regional precipitation, where precipitation lags discharge between 3–5 months ($R \sim 0.75$). Given most winter snowpack falls in December–March and peak streamflow subsequently occurs in May–June, the 3- to 5-month lead in peak correlations is consistent with wintertime snowpack and the subsequent spring melting (Collins et al. 1988; Hunter et al. 2006).

Figure 10 shows a scatterplot of the aggregate summer, spring, and the previous year's late fall precipitation with July–August discharge, depicting a strong relationship ($R = 0.79$). An estimated 65% of summer streamflow variability is related to the combined summertime precipitation (JA), spring (MAMJ), and the previous year's late fall (-ND) precipitation. The remaining 35% may be explained by other variables, such as temperature and antecedent soil moisture prior to precipitation (Woodhouse et al. 2016). We decompose the relative contributions of these seasonal precipitation anomalies on July–August discharge through a simple multiple linear regression model, where the predictand is July–August discharge, and the predictors are July–August, March–June, and November–December of the previous year precipitation anomalies. Based on the linear regression, contemporaneous precipitation anomalies in July–August explains an estimated 17%, which is slightly higher than past research ($\sim$ 10%) (Carroll et al. 2020).

The linear regression model also suggests an estimated 12% of July–August streamflow is due to the previous late fall's precipitation. This long-term memory of the upper Colorado River hydroclimate may be related to a positive relationship of fall soil moisture–spring discharge or building a healthy early snowpack is favorable for summertime discharge (Aziz et al. 2010; Bracken et al. 2010; Werner and Yeager 2013). Meanwhile, $\sim$ 35% of July–August streamflow is due to March–June precipitation. We do not include January–February precipitation in the regression

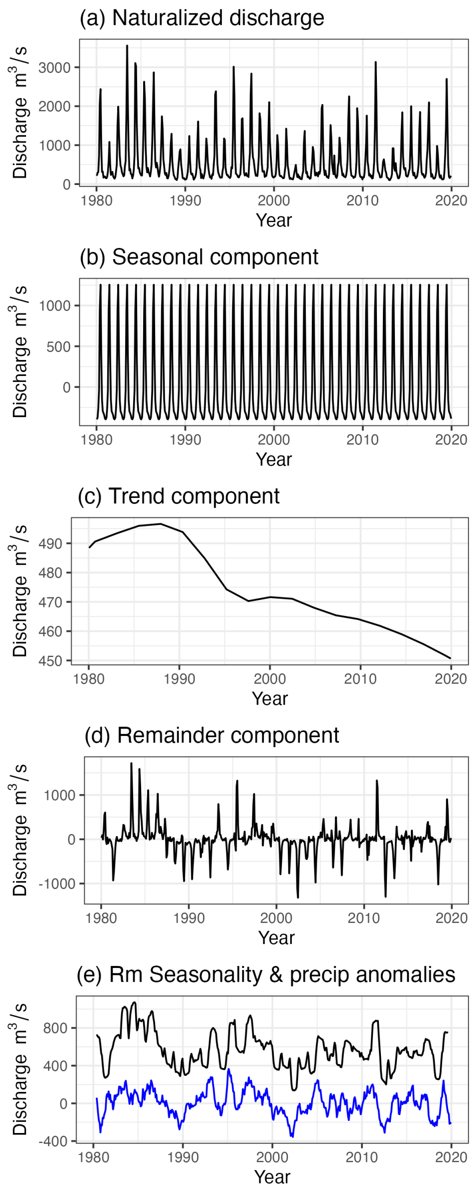

FIG. 9. (a) Naturalized monthly streamflow from 1980–2019. An additive decomposition is applied to obtain (b) the seasonal component, (c) long-term trends, (d) and the remainder component. The bottom (e) time series (black) represents the difference between the (b) seasonality component and (a) naturalized streamflow, resulting in only the (c) trend and (d) remainder components. The bottom (e) plot also depicts (blue) precipitation anomalies (mm/day) enhanced 700 times for visual purposes. A 5-month running mean is applied for both time series in 9e.

model because it was not statistically significant with July–August discharge ($R = 0.13, P = 0.451$).

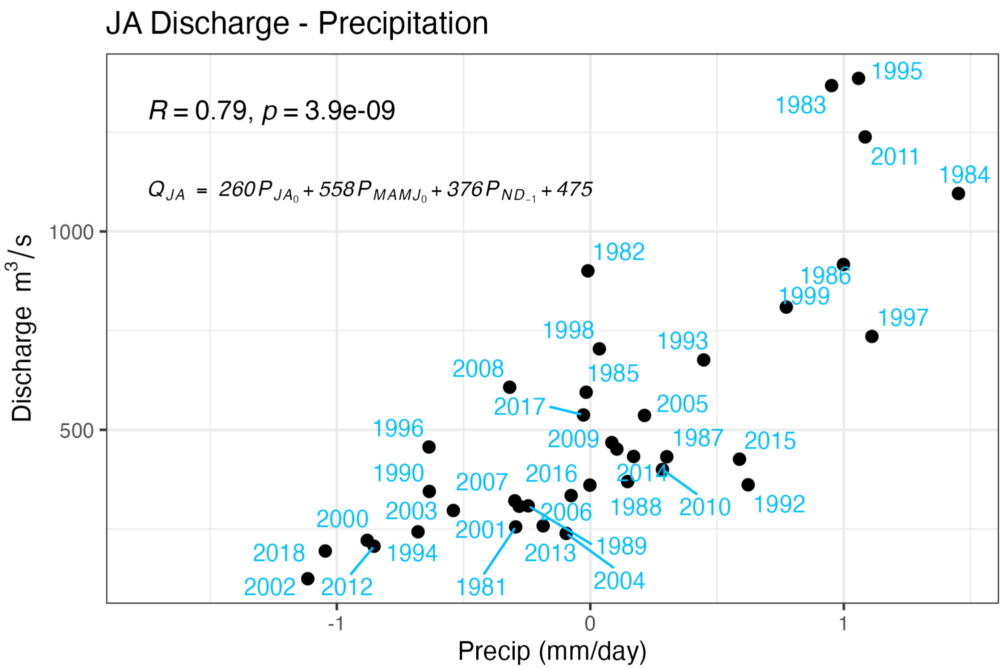

FIG. 10. Scatterplot of the combined July–August, March–June, and November-December of the previous year precipitation anomalies and July–August streamflow at the Lee's Ferry gauge. Precipitation is constrained to the upper Colorado River basin outlined in Figure 1. The relative contributions are shown via a linear regression of July–August, March–June, and November-December of the previous year's precipitation anomalies on July–August streamflow. The P-values for these three predictors are 0.043, < 0.001, and 0.001, respectively.

Wintertime precipitation is obviously important for spring streamflow, but simply not statistically significant for summertime streamflow in the regression model.

Based on the contemporaneous precipitation dependencies on streamflow, we look specifically at the synoptic patterns of the southwestern ridge of high pressure in Figure 11. When the ridge of high pressure is east of its climatological position favoring wet monsoon days (19.2% of July–August days), river discharge tends to increase ($R = 0.43$; $p = 0.007$). When the ridge of high pressure is northwest of its climatological position favoring dry days (20.7% of July–August days), discharge decreases ($R = -0.44$; $p = 0.005$). For days exhibiting other synoptic patterns, no statistically significant relationship exists with respect to discharge rates. While the number of days characterized by wet clusters is significantly related to July–August discharge, a number of notable outliers exist. For example, the discharge in 2000 and 2002 is notably low even though the relative number of wet and neutral days was above the norm (Fig. 11a and 7). As summer precipitation is

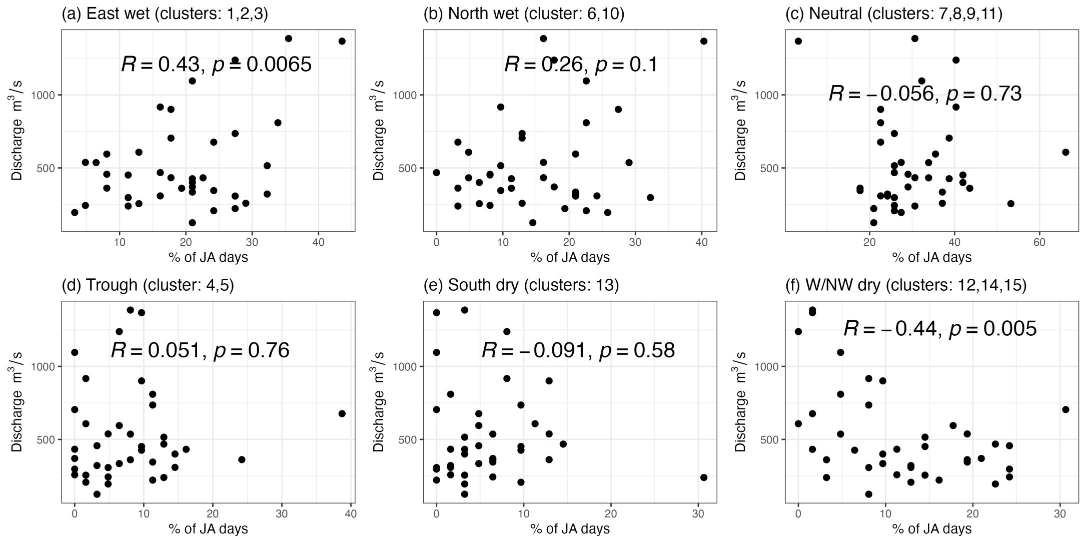

FIG. 11. July–August discharge at Lee's Ferry and the percentage of July–August days exhibiting a certain ridge of high pressure position based on Figure 7. The correlations and P-values are displayed for each subplot.

not the dominant modulator of summer discharge in a snowpack-dominated hydrological system, this spread is to be expected.

b. Raw daily streamflow

Lastly, we examine raw daily streamflow data to determine whether it supports the monthly naturalized streamflow analysis above. When we aggregate raw daily streamflow in July–August and compare it to July–August naturalized streamflow, we find a correlation of 0.69, significant above the 99.9% value. Figure S4 shows density plots of the lagged 5-day mean Colorado discharge (days 0–4) for each cluster's day (day 0). Clusters 1–6 favoring wetting 500 hPa patterns, have discharge densities skewing towards higher streamflow compared to clusters 9–15 favoring drying patterns. This is evident in the 90th percentile lines being further to the right for wet patterns. Clusters favoring dry patterns typically had reduced skewness to the right, favoring Gaussian distributions. Clusters 1–5 favoring a wetting pattern, show a mean discharge rate of 495.5 m^3/s whereas clusters 12–15 favoring a dry pattern show a mean discharge rate of 456.2 m^3/s, with a July–August 1980–2020 mean of 475.4 m^3/s. These results, combined with results using monthly naturalized streamflow, provide evidence that discharge rates of the upper Colorado River have dependencies on daily monsoon rains based on the positive precipitation that feeds into the Colorado

River. We recognize that any analysis with raw daily data is highly provisional, but we present the daily raw analysis as it supports the more robust monthly naturalized streamflow analysis.

6. Discussion and conclusion

This study examined synoptic patterns of the southwestern United States mid-tropospheric ridge of high pressure that contributes to a wet or dry North American Monsoon (NAM) by applying a k-means clustering analysis to 500 hPa geopotential height field. We assessed these synoptic patterns to changes in naturalized Colorado River streamflow and to climate variability. The primary results are:

1. The southwestern ridge of high pressure exhibits significant variability in its structure, strength, and location during summer.
2. An eastward or northward shift of the mid-tropospheric ridge of high pressure promotes increased precipitation during July–August over the Desert Southwest and the upper Colorado River basin accounting for 35% of days.
3. A southward or northwestward shift in the mid-tropospheric ridge of high pressure inhibits precipitation during July–August in the upper Colorado River basin accounting for 26% days.
4. Tropical Pacific and Pacific Meridional Mode cooling favor synoptic patterns consisting of an eastward shift in the ridge of high pressure that promotes wet days.
5. Eastern Tropical Pacific warming favors synoptic patterns consisting of a southward shift in the ridge of high pressure that promotes dry days.
6. Summertime monsoon rains contribute 17% of July–August streamflow variability in the upper Colorado River.
7. An eastward shift in the ridge of high pressure favors increased upper Colorado River discharge, whereas a west or northwest shift in the ridge of high pressure favors decreased discharge.

This study found 15 k-means characterizing changes in the structure, location, and intensity of the 500 hPa ridge of high pressure over the southwestern United States. Past research shows this ridge of high pressure is linked to NAM efficiency (Wang et al. 2011; Cerezo-Mota et al. 2011; Favors and Abatzoglou 2013; Seastrand et al. 2015). A synoptic pattern favoring wet days in the upper

Colorado River basin accompanies an eastward or northward shift in the 500 hPa ridge of high pressure or troughing, accounting for 42.7% of all July–August days in 1980–2020. A significant increase in atmospheric moisture accompanies these 500 hPa patterns for wet days. When lower-tropospheric winds curve from southeasterly to southwesterly around the western periphery of the ridge of high pressure over Baja California, integrated atmospheric moisture markedly increased over the upper Colorado River basin and the southwestern United States, suggesting a moisture source from the warm waters in Baja California. When lower-tropospheric winds are easterly from the Gulf of Mexico turning southeasterly over west Texas and New Mexico, integrated atmospheric moisture also increases over the eastern portion of the Desert Southwest, suggesting a potential moisture source from the Gulf of Mexico.

A synoptic pattern favoring dry days over the upper Colorado River basin accompanies a southward or northwestward shift of the 500 hPa ridge of high pressure, accounting for 26.3% of July–August days. This pattern deviates atmospheric moisture toward the west over California and the adjacent Pacific Ocean or keeps it to the south. Typically, over the upper Colorado River basin, the southward, west, or northwestward shift in the ridge of high pressure accompanies northwesterlies over the upper Colorado River basin promoting regional dry air and an inhibiting wind pattern from the Gulf of California and the Gulf of Mexico moisture sources.

For summers where we had synoptic patterns favoring more wet days, tropical Pacific and Pacific Meridional mode cooling accompanied an eastward shift in the ridge of high pressure. In contrast, eastern tropical Pacific El Niño-like warming accompanies a southward shift of the ridge of high pressure. Related to these variations in the ridge of high pressure, a Rossby wave train pattern emerges over the North Pacific, suggesting a tropical Pacific teleconnection. When the ridge of high pressure is north or northwest of its climatological position, no apparent climate variability is seen in composite analyses. Alternatively, when the MJO is in its active phase in the Indian Ocean, it contributes to increased monsoon rains in Mexico. Toward the north, our analysis indicates precipitation in the upper Colorado River basin does not have dependencies on any MJO phase. Because this is an analysis based on historical data, we would require a climate model experiment to assess the remote effect of ocean-atmosphere interactions on the southwestern ridge of high pressure in future studies. Our analysis linking these synoptic patterns to climate variability finds statistically significant correlations, but it must be noted that there is significant autocorrelation in climate variability, resulting in reduced effective degrees of freedom (Bretherton et al. 1999).

Past research has found a small effect of the NAM on streamflow variability (~ 10%), with our study finding that July–August precipitation contributes to an estimated 17% of July–August streamflow variability through a linear perspective (Carroll et al. 2020). Interestingly, our study found that discharge at Lee's Ferry, Arizona also has dependencies on springtime and the previous late fall's precipitation. Our analysis shows that seasons favoring days when the ridge of high pressure is east of its climatological position may promote increased discharge rates. In contrast, when the ridge of high pressure is northwest of its climatological position, our results suggest decreased discharge rates.

Our analysis does not consider tropical cyclone (TC) activity in the eastern North Pacific basin, but past research suggests a significant portion of NAM moisture plumes may stem from TC activity (Wayne Higgins et al. 2003), possibly connected to an active MJO phase (Lorenz and Hartmann 2006). Given ridge of high pressure structure, strength, and location may modulate the large-scale steering flow, and the TC tracks embedded within that flow, our k-means clustering method may capture changes in TC tracks and its associated moisture (George and Gray 1977; Zhao and Wu 2014; Johnson et al. 2022). For instance, when the ridge of high pressure placement is east of its climatological position, TCs and their associated moisture may recurve around the western periphery of the mid-tropospheric high, leading to increased moisture over the southwestern United States. Future studies should quantify TC track dependencies on ridge of high pressure placement, emphasizing moisture advection.

While the "elbow" and silhouette methods indicate the optimal k number of clusters is 12–15 (see methods), several of the clusters look similar to each other with only slight variations in spatial structure in the mid-tropospheric ridge of high pressure. These cluster do not suggest distinct modes of variability but rather classify days where the ridge of high pressure structure, intensity, and position are similar to one another. When we apply the k-means only to July Z500, the "elbow" and silhouette methods suggest the optimal k clusters is 8. When we apply the k-means to the first half of the data (i.e., 1980–2000 instead of 1980–2020), the "elbow" and silhouette methods indicate the optimal number of k clusters is 14. While the classification of the ridge of high pressure shows some differences when changing the data time period, similar results are found regarding the ridge of high pressure location on precipitation. The k-means method can erroneously find clusters even in smooth data, possibly in synoptic patterns that show gradual transitions rather than distinct, separable patterns (Singh et al. 2011). Alternative methods to classify and quantify the summertime synoptic patterns may be more suitable, such as self-organizing maps, eigenvector techniques such as empirical orthogonal functions or singular value decomposition, or simply, indices quantifying the ridge location.

About 10–40% of annual precipitation falls during July–August over the southwestern United States. While snowpack melt is the primary contributor to increased streamflow rates in spring and early summer, precipitation from the NAM also appears to be important for Colorado River discharge based on historical analysis, contributing an estimated 17% change in summertime streamflow variability. A tight connection between soil moisture and monsoon strength has been observed through a positive soil moisture – monsoon precipitation feedback mechanism and our study also supports this past research (Vivoni et al. 2008; Méndez-Barroso et al. 2009; Zhu et al. 2009). Monsoon rains can also contribute to healthy, moist soil for the subsequent winter snow-pack, which has an effect on following spring runoff efficiency, with our analysis capturing similar results. As a result, a tight, multi-seasonal hydroclimate interconnection between ocean-atmosphere effects, land-atmosphere interactions, monsoon strength, snowpack, spring runoff, and Colorado River discharge challenges scientists to better understand the Western United States hydroclimate (Gochis et al. 2010; Notaro and Zarrin 2011). Future studies should assess NAM dependencies on climate variability through physical modeling perspectives and further quantify its effect on streamflow, given the massive water resource issues plaguing the western United States.

Acknowledgments. ZFJ was supported by start-up support at Central Michigan University. We would like to express our sincere gratitude to the three anonymous reviewers whose insightful comments and suggestions significantly improved the quality of this manuscript.

Data availability statement. All data used in this study can be obtained free of charge to any member of the public. COBE-SST, CMAP, and NCEP data can be obtained from NOAA/OAR/ESRL PSD, Boulder, Colorado, USA. ERA5 can be obtained from ECMWF Copernicus. All analyses and plotting were performed using the NCAR command language (NCL) and R. The code in this study can be requested from the corresponding author.

References

Adams, D. K., and A. C. Comrie, 1997: The north american monsoon. *Bulletin of the American Meteorological Society*, **78 (10)**, 2197–2214.

Arritt, R. W., D. C. Goering, and C. J. Anderson, 2000: The north american monsoon system in the hadley centre coupled ocean-atmosphere gcm. *Geophysical Research Letters*, **27 (4)**, 565–568.

Aziz, O. A., G. A. Tootle, S. T. Gray, and T. C. Piechota, 2010: Identification of pacific ocean sea surface temperature influences of upper colorado river basin snowpack. *Water Resources Research*, **46 (7)**.

Barlow, M., S. Nigam, and E. H. Berbery, 1998: Evolution of the north american monsoon system. *Journal of Climate*, **11 (9)**, 2238–2257.

Bieda, S. W., C. L. Castro, S. L. Mullen, A. C. Comrie, and E. Pytlak, 2009: The relationship of transient upper-level troughs to variability of the north american monsoon system. *Journal of Climate*, **22 (15)**, 4213–4227.

Bizuneh, B. B., M. A. Moges, B. G. Sinshaw, and M. S. Kerebih, 2021: Swat and hbv models' response to streamflow estimation in the upper blue nile basin, ethiopia. *Water-Energy Nexus*, **4**, 41–53.

Bracken, C., B. Rajagopalan, and J. Prairie, 2010: A multisite seasonal ensemble streamflow forecasting technique. *Water Resources Research*, **46 (3)**.

Bretherton, C. S., M. Widmann, V. P. Dymnikov, J. M. Wallace, and I. Bladé, 1999: The effective number of spatial degrees of freedom of a time-varying field. *Journal of climate*, **12 (7)**, 1990–2009.

Brown, P. M., and R. Wu, 2005: Climate and disturbance forcing of episodic tree recruitment in a southwestern ponderosa pine landscape. *Ecology*, **86 (11)**, 3030–3038.

Carroll, R. W., D. Gochis, and K. H. Williams, 2020: Efficiency of the summer monsoon in generating streamflow within a snow-dominated headwater basin of the colorado river. *Geophysical Research Letters*, **47 (23)**, e2020GL090 856.

Castro, C. L., T. B. McKee, and R. A. Pielke, 2001: The relationship of the north american monsoon to tropical and north pacific sea surface temperatures as revealed by observational analyses. *Journal of Climate*, **14 (24)**, 4449–4473.

Cavadias, G., 1994: Detection and modeling of the impact of climatic change on river flows. *Engineering Risk in Natural Resources Management: With Special References to Hydrosystems under Changes of Physical or Climatic Environment*, Springer, 207–218.

Cerezo-Mota, R., M. Allen, and R. Jones, 2011: Mechanisms controlling precipitation in the northern portion of the north american monsoon. *Journal of Climate*, **24 (11)**, 2771–2783.

Chen, M., W. Shi, P. Xie, V. B. Silva, V. E. Kousky, R. Wayne Higgins, and J. E. Janowiak, 2008: Assessing objective techniques for gauge-based analyses of global daily precipitation. *Journal of Geophysical Research: Atmospheres*, **113 (D4)**.

Chiang, J. C., and D. J. Vimont, 2004: Analogous pacific and atlantic meridional modes of tropical atmosphere–ocean variability. *Journal of Climate*, **17 (21)**, 4143–4158.

Chikamoto, Y., S.-Y. S. Wang, M. Yost, L. Yocom, and R. R. Gillies, 2020: Colorado river water supply is predictable on multi-year timescales owing to long-term ocean memory. *Communications Earth & Environment*, **1 (1)**, 1–11.

Cleveland, R. B., W. S. Cleveland, J. E. McRae, and I. Terpenning, 1990: Stl: A seasonal-trend decomposition. *J. Off. Stat*, **6 (1)**, 3–73.

Collins, D., N. Doesken, and W. Stanton, 1988: Colorado floods and droughts. *National Water Summary*, **89**, 207–214.

Cook, B. I., T. R. Ault, and J. E. Smerdon, 2015: Unprecedented 21st century drought risk in the american southwest and central plains. *Science Advances*, **1 (1)**, e1400 082.

Cook, E. R., R. Seager, R. R. Heim Jr, R. S. Vose, C. Herweijer, and C. Woodhouse, 2010: Megadroughts in north america: Placing ipcc projections of hydroclimatic change in a long-term palaeoclimate context. *Journal of Quaternary Science*, **25 (1)**, 48–61.

D'Arrigo, R. D., and G. C. Jacoby, 1991: A 1000-year record of winter precipitation from northwestern new mexico, usa: a reconstruction from tree-rings and its relation to el niño and the southern oscillation. *The Holocene*, **1 (2)**, 95–101.

Demaria, E. M., P. Hazenberg, R. L. Scott, M. B. Meles, M. Nichols, and D. Goodrich, 2019: Intensification of the north american monsoon rainfall as observed from a long-term high-density gauge network. *Geophysical Research Letters*, **46 (12)**, 6839–6847.

Diem, J. E., and D. P. Brown, 2009: Relationships among monsoon-season circulation patterns, gulf surges, and rainfall within the lower colorado river basin, usa. *Theoretical and applied climatology*, **97**, 373–383.

Douglas, M. W., 1995: The summertime low-level jet over the gulf of california. *Monthly Weather Review*, **123 (8)**, 2334–2347.

Douglas, M. W., R. A. Maddox, K. Howard, and S. Reyes, 1993: The mexican monsoon. *Journal of Climate*, **6 (8)**, 1665–1677.

Erb, M., J. Emile-Geay, G. Hakim, N. Steiger, and E. Steig, 2020: Atmospheric dynamics drive most interannual us droughts over the last millennium. *Science advances*, **6 (32)**, eaay7268.

Erfani, E., and D. Mitchell, 2014: A partial mechanistic understanding of the north american monsoon. *Journal of Geophysical Research: Atmospheres*, **119 (23)**, 13–096.

Favors, J. E., and J. T. Abatzoglou, 2013: Regional surges of monsoonal moisture into the southwestern united states. *Monthly weather review*, **141 (1)**, 182–191.

Finch, Z. O., and R. H. Johnson, 2010: Observational analysis of an upper-level inverted trough during the 2004 north american monsoon experiment. *Monthly weather review*, **138 (9)**, 3540–3555.

Franzen, S. E., M. A. Farahani, and A. E. Goodwell, 2020: Information flows: Characterizing precipitation-streamflow dependencies in the colorado headwaters with an information theory approach. *Water Resources Research*, **56 (10)**, e2019WR026 133.

Fuller, R. D., and D. J. Stensrud, 2000: The relationship between tropical easterly waves and surges over the gulf of california during the north american monsoon. *Monthly weather review*, **128 (8)**, 2983–2989.

George, J. E., and W. M. Gray, 1977: Tropical cyclone recurvature and nonrecurvature as related to surrounding wind-height fields. *Journal of Applied Meteorology (1962-1982)*, 34–42.

Gochis, D. J., E. R. Vivoni, and C. J. Watts, 2010: The impact of soil depth on land surface energy and water fluxes in the north american monsoon region. *Journal of Arid Environments*, **74 (5)**, 564–571.

Gong, X., and M. B. Richman, 1995: On the application of cluster analysis to growing season precipitation data in north america east of the rockies. *Journal of climate*, **8 (4)**, 897–931.

Govender, P., and V. Sivakumar, 2020: Application of k-means and hierarchical clustering techniques for analysis of air pollution: A review (1980–2019). *Atmospheric pollution research*, **11 (1)**, 40–56.

Hales Jr, J. E., 1972: Surges of maritime tropical air northward over the gulf of california. *Monthly Weather Review*, **100 (4)**, 298–306.

Hartigan, J. A., and M. A. Wong, 1979: Algorithm as 136: A k-means clustering algorithm. *Journal of the royal statistical society. series c (applied statistics)*, **28 (1)**, 100–108.

Hersbach, H., 2016: The era5 atmospheric reanalysis. *AGU fall meeting abstracts*, Vol. 2016, NG33D–01.

Higgins, R., Y. Yao, and X. Wang, 1997: Influence of the north american monsoon system on the us summer precipitation regime. *Journal of climate*, **10 (10)**, 2600–2622.

Higgins, R. W., Y. Chen, and A. V. Douglas, 1999: Interannual variability of the north american warm season precipitation regime. *Journal of Climate*, **12 (3)**, 653–680.

Houze Jr, R. A., 2004: Mesoscale convective systems. *Reviews of Geophysics*, **42 (4)**.

Houze Jr, R. A., 2018: 100 years of research on mesoscale convective systems. *Meteorological Monographs*, **59**, 17–1.

Hrachowitz, M., H. Savenije, T. Bogaard, D. Tetzlaff, and C. Soulsby, 2013: What can flux tracking teach us about water age distribution patterns and their temporal dynamics? *Hydrology and Earth System Sciences*, **17 (2)**, 533–564.

Hu, H., and F. Dominguez, 2015: Evaluation of oceanic and terrestrial sources of moisture for the north american monsoon using numerical models and precipitation stable isotopes. *Journal of Hydrometeorology*, **16 (1)**, 19–35.

Hunter, T., G. Tootle, and T. Piechota, 2006: Oceanic-atmospheric variability and western us snowfall. *Geophysical Research Letters*, **33 (13)**.

Ishii, M., A. Shouji, S. Sugimoto, and T. Matsumoto, 2005: Objective analyses of sea-surface temperature and marine meteorological variables for the 20th century using icoads and the kobe collection. *International Journal of Climatology: A Journal of the Royal Meteorological Society*, **25 (7)**, 865–879.

Jain, A. K., 2010: Data clustering: 50 years beyond k-means. *Pattern recognition letters*, **31 (8)**, 651–666.

Johnson, Z. F., D. R. Chavas, and H. A. Ramsay, 2022: Statistical framework for western north pacific tropical cyclone landfall risk through modulation of the western pacific subtropical high and enso. *Journal of Climate*, **35 (22)**, 3787–3800.

Jolliffe, I. T., and A. Philipp, 2010: Some recent developments in cluster analysis. *Physics and Chemistry of the Earth, Parts A/B/C*, **35 (9-12)**, 309–315.

Kim, T.-W., C. Yoo, and J.-H. Ahn, 2008: Influence of climate variation on seasonal precipitation in the colorado river basin. *Stochastic Environmental Research and Risk Assessment*, **22 (3)**, 411–420.

Kodinariya, T. M., P. R. Makwana, and Coauthors, 2013: Review on determining number of cluster in k-means clustering. *International Journal*, **1 (6)**, 90–95.

Lorenz, D. J., and D. L. Hartmann, 2006: The effect of the mjo on the north american monsoon. *Journal of Climate*, **19 (3)**, 333–343.

Mankin, J., I. Simpson, A. Hoell, R. Fu, J. Lisonbee, A. Sheffield, and D. Barrie, 2021: Noaa drought task force report on the 2020–2021 southwestern us drought. *NOAA Drought Task Force, MAPP, and NIDIS*.

Mazon, J. J., C. L. Castro, D. K. Adams, H.-I. Chang, C. M. Carrillo, and J. J. Brost, 2016: Objective climatological analysis of extreme weather events in arizona during the north american monsoon. *Journal of Applied Meteorology and Climatology*, **55 (11)**, 2431–2450.

McCabe, G. J., D. M. Wolock, C. A. Woodhouse, G. T. Pederson, S. A. McAfee, S. Gray, and A. Csank, 2020: Basinwide hydroclimatic drought in the colorado river basin. *Earth Interactions*, **24 (2)**, 1–20.

McCann, J. F., 2010: *Synoptic circulation of the north american monsoon system and precipitation within the lower Colorado river basin*. Louisiana State University and Agricultural & Mechanical College.

Méndez-Barroso, L. A., E. R. Vivoni, C. J. Watts, and J. C. Rodríguez, 2009: Seasonal and interannual relations between precipitation, surface soil moisture and vegetation dynamics in the north american monsoon region. *Journal of hydrology*, **377 (1-2)**, 59–70.

Milligan, G. W., and M. C. Cooper, 1985: An examination of procedures for determining the number of clusters in a data set. *Psychometrika*, **50**, 159–179.

Moges, E., B. L. Ruddell, L. Zhang, J. M. Driscoll, and L. G. Larsen, 2022: Strength and memory of precipitation's control over streamflow across the conterminous united states. *Water Resources Research*, **58 (3)**, e2021WR030 186.

Notaro, M., and A. Zarrin, 2011: Sensitivity of the north american monsoon to antecedent rocky mountain snowpack. *Geophysical Research Letters*, **38 (17)**.

Orth, R., and S. I. Seneviratne, 2013: Propagation of soil moisture memory to streamflow and evapotranspiration in europe. *Hydrology and Earth System Sciences*, **17 (10)**, 3895–3911.

Pederson, N., and Coauthors, 2012: A long-term perspective on a modern drought in the american southeast. *Environmental Research Letters*, **7 (1)**, 014 034.

Peltier, D. M., and K. Ogle, 2019: Legacies of la niña: North american monsoon can rescue trees from winter drought. *Global change biology*, **25 (1)**, 121–133.

Prairie, J., and R. Callejo, 2005: Natural flow and salt computation methods. *US Department of the Interior USDOI, Bureau of Reclamation*.

Rousseeuw, P. J., 1987: Silhouettes: a graphical aid to the interpretation and validation of cluster analysis. *Journal of computational and applied mathematics*, **20**, 53–65.

Sagarika, S., A. Kalra, and S. Ahmad, 2016: Pacific ocean sst and z500 climate variability and western us seasonal streamflow. *International Journal of Climatology*, **36 (3)**, 1515–1533.

Seager, R., M. Hoerling, S. Schubert, H. Wang, B. Lyon, A. Kumar, J. Nakamura, and N. Henderson, 2015: Causes of the 2011–14 california drought. *Journal of Climate*, **28 (18)**, 6997–7024.

Seastrand, S., Y. Serra, C. Castro, and E. Ritchie, 2015: The dominant synoptic-scale modes of north american monsoon precipitation. *International Journal of Climatology*, **35 (8)**, 2019–2032.

Singh, K., D. Malik, N. Sharma, and Coauthors, 2011: Evolving limitations in k-means algorithm in data mining and their removal. *International Journal of Computational Engineering & Management*, **12 (1)**, 105–109.

Stuivenvolt-Allen, J., S.-Y. S. Wang, Z. Johnson, and Y. Chikamoto, 2021: Atmospheric rivers impacting northern california exhibit a quasi-decadal frequency. *Journal of Geophysical Research: Atmospheres*, **126 (15)**, e2020JD034 196.

Topping, D. J., J. C. Schmidt, and L. Vierra Jr, 2003: Computation and analysis of the instantaneous-discharge record for the colorado river at lees ferry, arizona—may 8, 1921, through september 30, 2000. Tech. rep., US Geological Survey.

U.S. Department of Interior, B. o. R., 1983: Draft colorado river simulation system hydrology data base. *Stochastic Environmental Research and Risk Assessment*.

U.S. Department of Interior, B. o. R., 2020: Colorado river basin natural flow and salt data.

Vaheddoost, B., and H. Aksoy, 2019: Reconstruction of hydrometeorological data in lake urmia basin by frequency domain analysis using additive decomposition. *Water Resources Management*, **33**, 3899–3911.

Vivoni, E. R., H. A. Moreno, G. Mascaro, J. C. Rodriguez, C. J. Watts, J. Garatuza-Payan, and R. L. Scott, 2008: Observed relation between evapotranspiration and soil moisture in the north american monsoon region. *Geophysical Research Letters*, **35 (22)**.

Wang, S.-Y., T.-C. Chen, and E. S. Takle, 2011: Climatology of summer midtropospheric perturbations in the us northern plains. part ii: Large-scale effects of the rocky mountains on genesis. *Climate dynamics*, **36 (7)**, 1221–1237.

Wayne Higgins, R., and Coauthors, 2003: Progress in pan american clivar research: the north american monsoon system. *Atmósfera*, **16 (1)**, 29–65.

Werner, K., and K. Yeager, 2013: Challenges in forecasting the 2011 runoff season in the colorado basin. *Journal of Hydrometeorology*, **14 (4)**, 1364–1371.

Williams, A. P., B. I. Cook, and J. E. Smerdon, 2022: Rapid intensification of the emerging southwestern north american megadrought in 2020–2021. *Nature Climate Change*, **12 (3)**, 232–234.

Woodhouse, C. A., G. T. Pederson, K. Morino, S. A. McAfee, and G. J. McCabe, 2016: Increasing influence of air temperature on upper colorado river streamflow. *Geophysical Research Letters*, **43 (5)**, 2174–2181.

Xie, P., M. Chen, and W. Shi, 2010: Cpc unified gauge-based analysis of global daily precipitation. *Preprints, 24th Conf. on Hydrology, Atlanta, GA, Amer. Meteor. Soc*, Vol. 2.

Xie, P., M. Chen, S. Yang, A. Yatagai, T. Hayasaka, Y. Fukushima, and C. Liu, 2007: A gauge-based analysis of daily precipitation over east asia. *Journal of Hydrometeorology*, **8 (3)**, 607–626.

Zhao, H., and L. Wu, 2014: Inter-decadal shift of the prevailing tropical cyclone tracks over the western north pacific and its mechanism study. *Meteorology and Atmospheric Physics*, **125 (1)**, 89–101.

Zhao, S., and J. Zhang, 2022: Causal effect of the tropical pacific sea surface temperature on the upper colorado river basin spring precipitation. *Climate Dynamics*, **58 (3-4)**, 941–959.

Zhu, C., L. R. Leung, D. Gochis, Y. Qian, and D. P. Lettenmaier, 2009: Evaluating the influence of antecedent soil moisture on variability of the north american monsoon precipitation in the coupled mm5/vic modeling system. *Journal of Advances in Modeling Earth Systems*, **1 (4)**.